Photocatalytic Nanolithography of Self-Assembled Monolayers and Proteins

Ehtsham Ul-Haq,[†,‡] Samson Patole,[‡,§] Mark Moxey,[‡] Esther Amstad,[∥] Cvetelin Vasilev,[§] C. Neil Hunter,[§] Graham J. Leggett,[‡,*] Nicholas D. Spencer,[∥] and Nicholas H. Williams[‡]

[‡]Department of Chemistry, University of Sheffield, Brook Hill, Sheffield S3 7HF, United Kingdom, [§]Department of Molecular Biology and Biotechnology, University of Sheffield, Western Bank, Sheffield S10 2TN, United Kingdom, and [∥]Laboratory for Surface Science and Technology, Department of Materials, ETH Zurich, Wolfgang-Pauli-Strasse 10, CH-8093 Zürich, Switzerland. [†]Present address: [†]Department of Chemical and Biological Engineering, The University of Sheffield, Mappin Street, Sheffield S1 3JD, U.K. (E.U.-H.).

ABSTRACT Self-assembled monolayers of alkylthiolates on gold and alkylsilanes on silicon dioxide have been patterned photocatalytically on sub-100 nm length-scales using both apertured near-field and apertureless methods. Apertured lithography was carried out by means of an argon ion laser (364 nm) coupled to cantilever-type near-field probes with a thin film of titania deposited over the aperture. Apertureless lithography was carried out with a helium–cadmium laser (325 nm) to excite titanium-coated, contact-mode atomic force microscope (AFM) probes. This latter approach is readily implementable on any commercial AFM system. Photodegradation occurred in both cases through the localized photocatalytic degradation of the monolayer. For alkanethiols, degradation of one thiol exposed the bare substrate, enabling refunctionalization of the bare gold by a second, contrasting thiol. For alkylsilanes, degradation of the adsorbate molecule provided a facile means for protein patterning. Lines were written in a protein-resistant film formed by the adsorption of oligo(ethylene glycol)-functionalized trichlorosilanes on glass, leading to the formation of sub-100 nm adhesive, aldehyde-functionalized regions. These were derivatized with aminobutylnitrilotriacetic acid, and complexed with Ni^{2+}, enabling the binding of histidine-labeled green fluorescent protein, which yielded bright fluorescence from 70-nm-wide lines that could be imaged clearly in a confocal microscope.

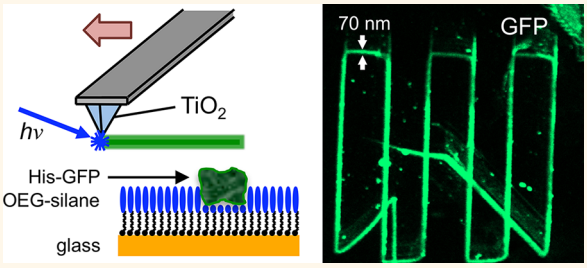

KEYWORDS: nanofabrication · photocatalytic patterning · near-field lithography · local probe lithography · protein patterning · GFP · monolayers

Nanofabrication is a key underpinning technology in nanoscience. Self-assembled monolayers (SAMs)[1−4] provide a powerful and versatile means by which to control interfacial molecular structure and interactions, and the modification of SAMs at nanometer length scales has attracted widespread attention during the past two decades.[5] A variety of approaches has been developed, including dip-pen nanolithography,[6−12] nanoshaving, and nanografting,[13−15] local oxidation,[16,17] electron beam lithography,[18−21] microcontact printing,[22−24] and scanning near-field lithography (SNP),[25−29] all of which have been employed successfully to pattern SAMs at better than 100 nm resolution.

The control of protein organization on sub-100 nm length scales presents particular challenges.[9,20,23,30−40] Proteins are able to adsorb strongly to most surfaces, because they display a wide variety of functional groups (charged and uncharged, cationic and anionic, hydrophilic and hydrophobic) and because they exhibit substantial conformational freedom. The first requirement for protein patterning is thus an effective means to control nonspecific adsorption. A number of approaches have been reported in the literature, but the most widely used ones have been based around poly(ethylene glycol)[41] and its derivatives, including oligo(ethylene glycol) (OEG)-terminated SAMs,[42−48] plasma-polymerized films,[49−51] and poly(oligoethylene glycol methacrylate) brushes.[52−54]

One approach to protein patterning is to form a protein-resistant surface and then selectively introduce protein-binding regions. For example, protein-resistant OEG-functionalized nitrophenylethoxycarbonyl-protected silane films have been selectively deprotected by near-field optical methods to expose amine groups that may be

* Address correspondence to graham.leggett@sheffield.ac.uk.

Received for review April 24, 2013 and accepted August 23, 2013.

Published online August 23, 2013
10.1021/nn402063b

derivatized by biotin and then streptavidin,[40] and OEG-functionalized SAMs have been patterned by near-field lithography to create regions into which proteins may be introduced.[55−57] However, control of protein conformation following binding to a surface remains challenging: not only is it difficult to control the orientation of the biomolecule, but additionally, ensuring the retention of protein activity following immobilization on nanostructured surfaces is difficult because of the propensity for immobilized proteins to undergo conformational changes. Moreover, the choice of substrate can be important: biological systems are typically interrogated by optical techniques that rely on the transmission of light through a specimen; substrates such as gold and Si are problematic because of their opacity, and gold and other metals also quench fluorescence. Glass is the ideal substrate for investigations of biological systems. Comparatively few examples exist in the literature of the site-specific localization on nanometer-scale regions of proteins, accompanied with a demonstration of retention of conformation. One example is the use of near-field photodegradation of poly(ethylene glycol)-functionalized SAMs on glass by Reynolds *et al.*, who derivatized the patterned features with nitrilotriacetic acid and, after complexation with nickel, bound histidine-tagged yellow-fluorescent protein to the surface.[57]

The present study describes a simple generic method for patterning SAMs based on the photocatalytic degradation of adsorbates, in which a local probe, either an apertured scanning near-field optical microscope (SNOM) probe, or an AFM probe, coated with titania, is utilized to cause localized photodegradation. In the latter mode, the approach is capable of implementation on any commercial AFM system. The use of a photocatalytic lithographic process means that the approach is applicable to any substrate coated with an organic film.

The photocatalytic properties of titania are well-known[58−60] and are exploited in commercial applications such as self-cleaning glass.[58] When TiO_2 is illuminated by photons with energies equal to or greater than its band gap, the absorbed UV light excites electron−hole pairs in the TiO_2 layer, which react with oxygen molecules and water to generate highly reactive species, including hydroxyl radicals and excited oxygen species, which have strong oxidative power to decompose organic matter. Remote TiO_2 photocatalytic lithography has been used previously to degrade silane and thiol self-assembled monolayers[61−66] to obtain surface chemical gradients[61] and to pattern enzymes and cells on the surface. Recently, this technique was used for cutting graphene sheets into arbitrary shapes, layer by layer thinning of the multilayer graphene sheets, and local oxidation.[67] However, it has not been regarded previously as a nanofabrication tool. The novel step in the present work is the use

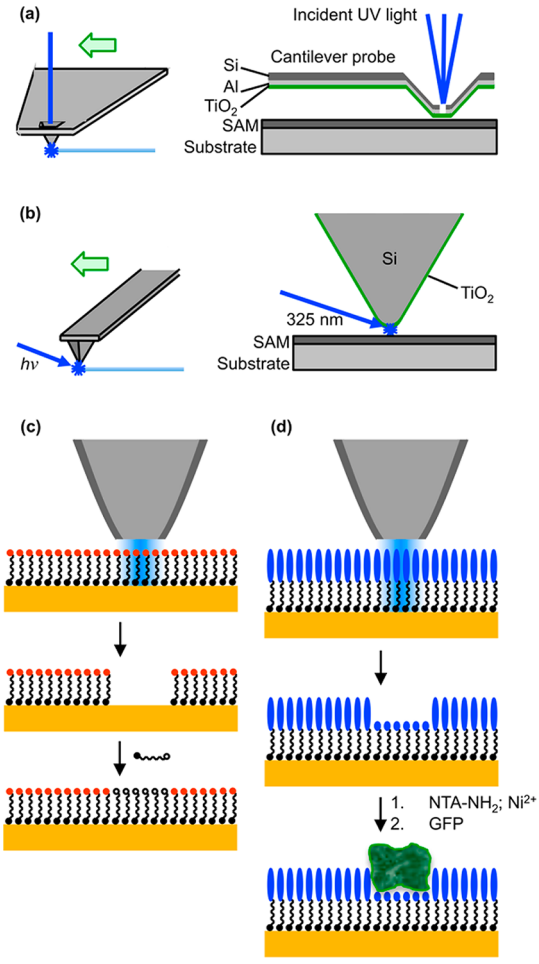

Figure 1. Schematic diagram showing the different approaches examined in this work. (a) A commercial cantilever SNOM probe, coated on its front face with titania, is illuminated from the back face by light from an HeCd laser. (b) Alternatively, a beam of light from an HeCd laser is directed onto the apex of a titania-coated AFM probe held in close proximity to a SAM. (c) Local exposure of a SAM of alkylthiolates leads to their degradation and enables their replacement by a second, contrasting thiolate in a solution-phase process. (d) Degradation of OEG-terminated silanes yields aldehyde functional groups, which bind nitrilotriacetic acid *via* an amine linker. Complexation of the surface with Ni^{2+} enables site-specific binding of His-tagged green fluorescent protein (GFP).

of a Ti-coated AFM probe to execute sub-100 nm patterning in a SAM. This important modification makes photocatalytic nanolithography possible on any commercial AFM system.

The experimental procedure is depicted schematically in Figure 1. Two alternate procedures were employed. In the first, light from a HeCd laser was incident on the back face of a subwavelength aperture in a SNOM probe that had been coated with a thin film of titania (formed by ambient oxidation of a thin Ti film). Electron−hole pair generation was initiated at the front face of the TiO_2 coating by the near-field associated with the aperture, leading to the localized creation of reactive species that could be used to pattern a SAM. In the alternate arrangement, an AFM

probe was coated with a thin film of Ti. After formation of the native oxide at the Ti surface by ambient oxidation, the probe was illuminated by light from the HeCd laser in close proximity to a SAM, leading to localized photocatalytic degradation of the organic layer. In both cases, annealing of the native oxide film was required, in order to form the catalytically active anatase phase; results were poor for probes that were not annealed. Here we report results obtained by both techniques during the degradation and replacement of alkylthiolates on gold, and during the selective degradation of protein-resistant OEG-terminated silane films on glass (Figure 1).

RESULTS AND DISCUSSION

Photopatterning of Alkylthiolate SAMs. Alkylthiolate SAMs were patterned by apertured photocatalytic nanolithography (PCN). The operation of the instrument in this mode is shown in Figure 1a, and the lithographic process is shown in the schematic in Figure 1c. The apertured probe, illuminated from above at 364 nm, was traced across the sample. Excitation of the titania film covering the aperture caused formation of reactive species beneath the aperture that caused photocatalytic modification of the alkylthiolate SAM, resulting in removal of adsorbates.

Figure 2a shows lateral force microscopy (LFM) images of a series of lines written into a carboxylic acid terminated SAM in this way, followed by immersion in a solution of dodecanethiol in ethanol. Figure 2b shows two lines at higher magnification, and a line section through one of the lines is shown in Figure 2c. The hydrophobic dodecanethiol molecules have adsorbed to regions of the surface from which the 11-mercaptoundecanoic acid has been removed by photocatalytic degradation. This gives rise to differential contrast over the two different regions of the surface: the friction force measured under ambient conditions over the hydrophobic SAM is smaller than that measured for the carboxylic acid functionalized adsorbates, so the lines exhibit darker contrast than the surrounding surface, because the friction force (proportional to the lateral deflection of the AFM probe) is smaller in these regions than in those where the carboxylic acid terminated thiolates are intact. The line width in Figure 2, determined as the full width at half-maximum height (fwhm) of a line section through the lateral force image, was 146 nm. The mean of 10 different features fabricated in the same way was 129 ± 11 nm. While the diameters of the apertures in the near-field probes were not measured routinely *after* Ti deposition, random samples of *uncoated* probes yielded aperture sizes of about 130 nm, suggesting that the feature size was limited by the aperture size in the probe.

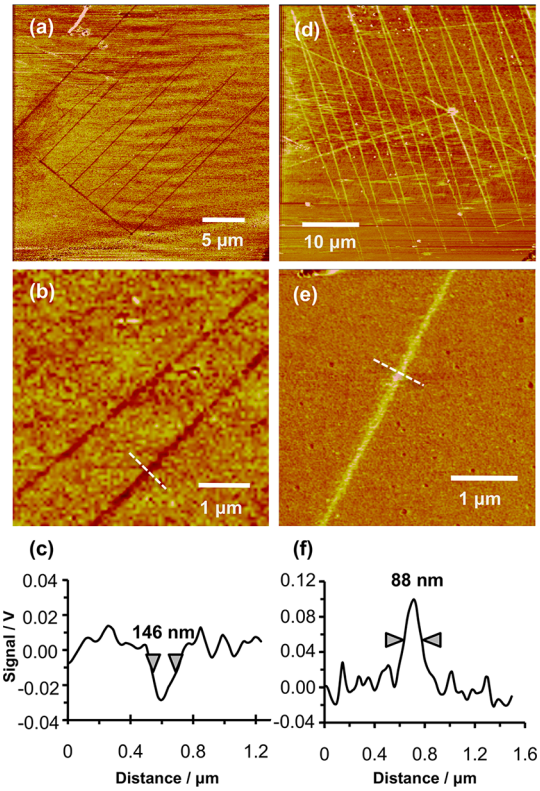

Figure 2. Lateral force microscopy image of an 11-mercaptoundecanoic acid SAM following patterning by apertured photocatalytic nanolithography and subsequent immersion in a dilute solution of dodecanethiol. (b) A region of image (a) at higher magnification, and (c) shows a line section acquired along the dashed line in (b). (d–f) Corresponding images acquired for a dodecanthiol SAM following photocatalytic nanolithography and immersion in a solution of 11-mercaptoundecanoic acid.

Figure 2d shows lines that have been formed in a SAM of dodecanethiol. The titania-coated aperture probe was translated across the monolayer, causing localized photocatalytic degradation of the methyl-terminated adsorbates. Following immersion of the sample in a solution of 11-mercaptoundecanoic acid in ethanol, the polar molecule adsorbs to the regions of bare gold created by degradation of dodecanethiol. In the lateral force image in Figure 2d, these carboxylic acid-functionalized regions exhibit brighter contrast than the surrounding methyl-terminated regions, consistent with the expected larger friction force for the polar SAM under ambient conditions. Figure 2e shows a region of the pattern in Figure 2d at higher magnification, and the accompanying line section (Figure 2f) reveals that sub-100 nm resolution is feasible, possibly as a result of partial occlusion of the aperture in the near-field probe by the Ti coating. The mean fwhm of 10 features fabricated in this way was 86 ± 10 nm.

The attainment of such high resolution was unexpected, because the reactive oxygen species formed at the titania surface by UV illumination are expected to be reasonably mobile. Diffusion of active species outside the area defined by the aperture in the near-field

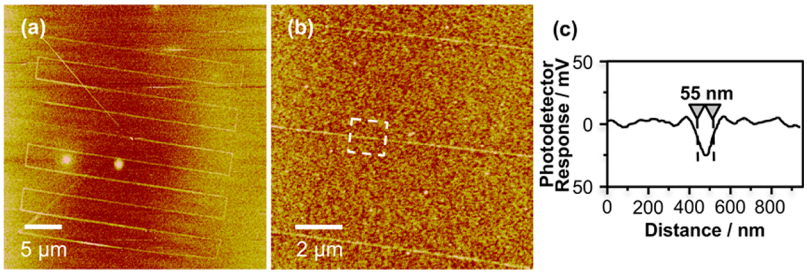

Figure 3. Lateral force microscopy images of features formed in an OEG-silane film by apertureless photocatalytic nanolithography (PCN). (a) Low-magnification image. (b) Higher magnification image of three lines shown in (a). (c) Section through one of the lines shown in (b), corresponding to the mean section along the segment of the line marked with a dashed box in (b).

probe might be expected to cause feature broadening. However, in this case, it is clear that no significant broadening has occurred. We speculate that active oxygen species are quickly deactivated by collisions with air molecules, reducing their effective range, and meaning that modification occurs only directly beneath the aperture.

In previous reports of scanning near-field photolithography by exposure to a near-field probe coupled to a frequency-doubled argon ion laser it was shown that excellent resolution could be achieved. However, a limitation was that the methodology relied upon the excitation of a very specific pathway. In the case of alkylthiolates, this was hot-electron excitation, leading to tunneling into an antibonding orbital of the adsorbate headgroup, a mechanism that was highly specific to the particular adsorbate/substrate combination under investigation. However, the present approach is entirely generic: because it relies upon the photocatalytic degradation of organic matter, it is, in principle, applicable to any film of organic molecules formed on any inorganic substrate.

To illustrate the generic nature of PCN, patterns were fabricated in a film of OEG-silane on glass. Moreover, rather than using an aperture probe, a titania-coated AFM probe was used as the excitation source in this case, as shown schematically in Figure 1b. The probe was brought into proximity with the silane film, and illuminated by a HeCd laser (325 nm) aligned at grazing incidence to the sample surface. The probe was translated across the sample surface, causing localized degradation of the adsorbates, and the sample was characterized by LFM.

Figure 3a shows a low-magnification image of a large area containing 10 lines approximately 25 μm long. Figure 3b shows three lines at higher magnification, and Figure 3c shows the mean section through a portion of one line (marked with a box), revealing an fwhm of only 55 nm. Line widths in the range 50−70 nm were achieved repeatably and the mean of 10 measurements on different structures was 63 ± 9 nm. Such high resolution was unexpected. As noted above, reactive oxygen species generated by electron−hole recombination mechanisms at the titania surface were expected to be capable of diffusion through the gas-phase, and an AFM probe represents an even less well-confined excitation source than an aperture. The explanation postulated above, that excited oxygen species may only diffuse short distances before collisional deactivation, seems apposite in the present case too; presumably the mean free path is sufficiently small that only organic groups that are close to the apex of the probe are degraded, and only a small area at the apex of the probe, in very close proximity with the surface, is able to cause significant degradation of the organic layer.

To fabricate the patterns shown in Figure 3, the probe was mounted in a WiTec α-SNOM near-field microscope, which has a convenient open architecture. However, the optical capabilities of the instrument were not utilized and it was simply used to scan the cantilever probe. It is anticipated that similar results could be achieved with any atomic force microscope that had a sufficiently open architecture to allow a laser beam to be directed at the tip−sample contact.

Although the features formed by PCN are clearly visible in Figure 3, the contrast between modified and virgin regions in the lateral force microscopy images is not strong. This was expected, based on previous work in this laboratory, which has shown that UV-degradation of OEG-silane films causes elimination of ethylene glycol groups and the formation of aldehyde and carboxylic acid functional groups.[57,68−70] The mechanism is thought to be similar to that for the photodegradation of OEG-functionalized thiols and polymers.[68,69] Because the OEG-silane is hydrophilic and has a lengthy and readily deformable oligo(ethylene glycol) chain, it exhibits a comparatively large friction coefficient; while this is increased by degradation of the EG chain, the magnitude of the change is modest. It was hypothesized that photocatalytic degradation may yield similar surface chemistries to those formed by other degradation processes, which have been shown to enable functionalization of oligo(ethylene glycol) type surfaces by aminobutylnitrilotriacetic acid (ABNTA) *via* the reaction between an amine on the

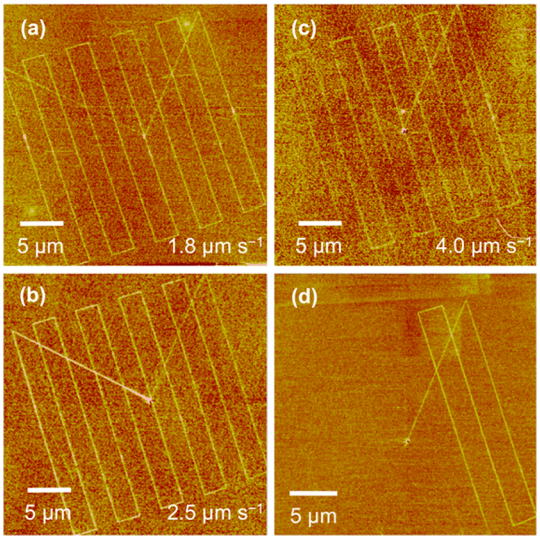

Figure 4. Lateral force microscopy images of features formed in OEG-silane films by apertureless PCN followed by conjugation of aminobutylnitrilotriacetic acid to the modified regions of the surface. (a–c) Patterns fabricated at different writing rates are shown, and (d) shows a pattern fabricated in an identical fashion to that in (a), but with the laser beam blanked after writing the first three lines.

ABNTA linker and aldehyde groups at the surface.[57] The patterns formed by apertureless photocatalytic degradation were treated with ABNTA, therefore, to yield an NTA-terminated surface for subsequent bioconjugation. It was hypothesized that the carboxylate groups on the NTA moiety would yield a high surface free energy, enhancing the contrast in lateral force images. Figure 4a shows a sample that, after nanolithography, has been cleaned by sonication in hexane and then functionalized with ABNTA. The contrast difference between the modified and virgin regions of the surface is enhanced relative to the images shown in Figure 3, confirming that the highly polar NTA functional groups provide an additional increase in the coefficient of friction measured for the modified regions of the surface as expected.

The effect of the writing rate on the lithographic process was also examined. Writing rates of between 1.8 and 4.0 μm s^{-1} were used. All samples were treated with ABNTA to enhance the contrast in lateral force microscopy. At 1.8 and 2.5 μm s^{-1} (Figure 4a and b, respectively) there was no significant difference in the continuity of the lines, the contrast difference between the features and the surrounding surface, or the line width (fwhm 75 $\pm$ 10 nm in Figure 4a and 84 $\pm$ 10 nm in Figure 4b). However, when the writing rate was increased to 4.0 μm s^{-1}, the contrast difference between the features and the surrounding surface weakened and the lines became discontinuous in places. The line width remained unaltered within the limits of experimental error (fwhm 99 $\pm$ 20 nm). Apertureless PCN thus appears unsuited to very high-speed processing but is capable of being implemented at rates comparable to those employed in most other types of local probe lithography that are used to pattern organic thin films. The apparent lack of a dependence of the feature size on the writing rate suggests that the lithographic process requires close proximity between the probe and the sample, so that the radius of curvature of the probe may have a strong effect on the resolution achievable.

To test that photocatalytic lithography was indeed being observed and not probe-induced mechanical modification of the surface, the laser beam was blanked regularly. Figure 4d shows an example of the behavior observed. The probe was initially located near the center of the region shown in Figure 4d, and moved diagonally toward the top right corner of the region. Three ~25 μm lines were written at a spacing of about 2.5 μm, before the laser was blanked after writing the third line (bottom right of Figure 4d). Writing was quickly extinguished.

The features shown in Figures 3 and 4 formed by apertureless PCN were functionalized with ABNTA, leading to enhanced friction contrast. Complexation of NTA-functionalized surfaces with Ni^{2+} enables binding of histidine-tagged proteins, a convenient surface bioconjugation strategy because of the ease with which His-tags may be introduced to many proteins using molecular biology techniques and because of the strength and specificity of their coordination to nickel–NTA complexes. In the present case, the feasibility of using apertureless PCN to form protein nanopatterns was investigated by writing features in an OEG-silane film, attaching ABNTA and complexing the surface with Ni^{2+}. The samples were imaged by lateral force microscopy to check feature sizes. The line widths were confirmed to be about 70 nm. The samples were then immersed in a solution of His-tagged green fluorescent protein (GFP) in buffer for 18 h and characterized by scanning laser confocal microscopy (Figure 5).

Figure 5a shows a low magnification micrograph of a ~300 $\times$ 300 μm^2 region containing, in the lower right quadrant of the image, a pattern fabricated by apertureless PCN. The remainder of the surface is dark, indicating an absence of nonspecific adsorption of protein, with the exception of a small number of bright points that probably result from the deposition of isolated proteins or small aggregates of protein. At low magnification, the narrow GFP features are just visible (Figure 5a). Figure 5b shows the pattern in Figure 5a at higher magnification. The lines fabricated by apertureless PCN are clearly visible against the dark background presented by the protein-resistant OEG-silane. Although the lines appear broadened in the fluorescence micrographs because of the resolution limit inherent in a conventional optical characterization tool, it is significant that the very bright contrast difference between the GFP-functionalized nanolines

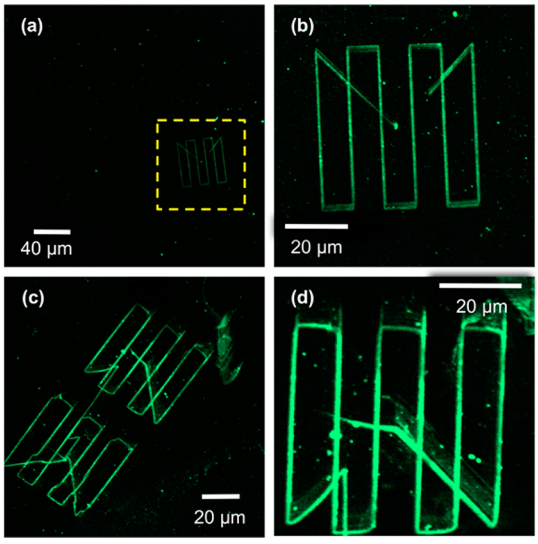

Figure 5. Confocal fluorescence microscopy images of samples that have been patterned using apertureless PCN, followed by conjugation with first ABNTA then nickel and His-tagged GFP. The region marked with a dashed box in (a) is shown at higher magnification in (b).

and the surrounding surface is being observed for features that are only 70 nm wide. This suggests that the density of attachment of the protein is high and also that the conformation of the protein is largely preserved following complexation to the surface (fluorescence in GFP is conformation-dependent[71,72]).

Figure 5c shows a second set of patterns fabricated by apertureless PCN, and Figure 5d shows the upper pattern at higher magnification. Very clear contrast is again observed between the nanolines, which exhibit strong fluorescence, and the OEG-silane surface, which predominantly exhibits a very dark contrast. A small number of bright points are observed that probably result from the deposition of isolated proteins or small aggregates of protein, together with a band of weak fluorescence running parallel to the long diagonal from the center of the pattern in Figure 5d to the lower right-hand corner. The origin of the latter feature is unclear, but the line results from the rapid motion of the cantilever from its initial rest point (the center of the patterned area) to the starting position for writing lines, and it is possible that torsion of the cantilever as a result causes a localized modification in the exposure mechanism, yielding a broader band of low-intensity modification. The majority of the isolated features are objects that are much smaller than the protein-functionalized lines. Given that those lines are at most 8–10 protein molecules wide, the majority of these isolated points are probably single molecules, their size determined by the point-spread function of the microscope. Three features are observable in the lower right-hand quandrant of Figure 5d that are slightly brighter, but they are still smaller than the main lithographic features, and they possibly represent small aggregates of molecules. This indicates, in general, an exceptionally low level of nonspecific adsorption given that at monolayer coverage the region shown in Figure 5d would contain some 10^7 proteins.

Fluorescence images could not be formed from patterns when the ABNTA attachment step was omitted from the process, suggesting that the protein binding was site-specific. When patterned, ABNTA-functionalized nanolines were immersed in solutions of His-GFP for short periods of time, there was little coupling of GFP to the surface. This suggests that degradation of the OEG-silane during the lithographic experiment was not complete; some intact OEG groups remained at the surface and conferred a measure of protein-resistance even after lithographic modification. Consequently, it was necessary to immerse the patterned samples in GFP solutions for lengthier time periods (overnight) to achieve extensive functionalization of the surface. Similar behavior, where a balance can be achieved between lithographic modification to enable the introduction of protein-binding functional groups and retention of resistance to nonspecific adsorption, has been reported previously for other PEGylated systems (including photodegradation of OEG-silanes and in the patterning of silanes protected with OEG-functionalized nitrophenyl groups).[40] For bioconjugation of nanostructures, this is an important benefit because it ensures that patterns result predominantly from site-specific immobilization through His–NTA interactions.

CONCLUSIONS

Photocatalytic nanolithography can be used to pattern organic thin films and monolayers at the nanoscale using either an apertured approach, in which a scanning near-field optical microscope probe is coated with a thin film of titania, or an apertureless approach, in which a titania-coated AFM probe is illuminated by a laser beam (HeCd laser, 325 nm) aligned orthogonal to the tip and at grazing incidence to the resist layer. Probes are fabricated easily by thermal evaporation of a thin Ti film and ambient oxidation to yield the oxide. Photocatalytic degradation enables the removal of alkylthiolates from gold surfaces and their replacement by contrasting alkylthiolates. OEG-silane films may be degraded to yield narrow features that, following complexation with aminobutyl nitrilotriacetic acid and Ni^{2+}, may be used to immobilize His-tagged green fluorescence protein. Although the photocatalytic process relies on the creation of excited oxygen species close to the titania surface, it is thought that the mean free paths of these species prior to deactivation by collision with air molecules are small, meaning that the photocatalytic process is highly localized. Consequently, feature sizes in the range 50–70 nm were achieved repeatably, even in apertureless photocatalytic nanolithography. A particularly attractive feature

of this approach is that it is feasible, in principle, on any atomic force microscope, provided it has sufficient optical access to enable direction of a laser beam at the probe.

METHODS

Dodecanethiol (98%), and 11-mercaptoundecanoic acid (98%) were obtained from Sigma Aldrich (Poole, UK) and used as received. Absolute ethanol (99.8+%) was obtained from Fisher Scientific. 2-[Methoxy(polyethyleneoxy)propyl]-trichlorosilane ($CH_3O(C_2H_4O)_{6-9}(CH_2)_3Cl_3Si$, henceforth, OEG-silane) was obtained from Fluorochem (Hadfield, U.K.).

All glassware used in the formation of SAMs was first cleaned by submersion in piranha solution, a mixture of 30% hydrogen peroxide and 95% concentrated sulfuric acid in the ratio 3:7 for at least 40 min. (*Caution: Piranha solution is an extremely strong oxidizing agent which has been known to detonate spontaneously upon contact with organic material.*) The glassware was rinsed thoroughly with deionized water (Elgar Nanopure, 18.2 MΩ) a minimum of six times and then sonicated for 10 min before being placed in the oven (approximately 80 °C) and left overnight to dry.

Substrates (glass slides/silicon wafers) were subjected to an additional cleaning step. Before submersion in piranha solution, they were first cut to size using a diamond-tipped scribe and then sonicated in toluene, acetone, and deionized water for 15 min, respectively. After treatment with piranha solution, the substrates were rinsed with deionized water and then submerged in the RCA (Radio Cooperative America) type 1 cleaning solution, a 1:1:5 mixture of 30% hydrogen peroxide, ammonium hydroxide (28−30% NH_3 basis), and deionized water at 80 °C. The substrates were then rinsed thoroughly before being placed in the oven to dry.

The substrates for formation of alkanethiolate self-assembled monolayers were prepared by evaporating 5 nm Cr and 20 nm Au onto clean glass microscope slides. The substrates were immersed in a 1 mM solution of appropriate thiol (dodecanethiol or 11-mercaptoundecanoic acid) in ethanol for 24 h. The substrates were then rinsed in clean ethanol repeatedly and dried with nitrogen.

The substrates for PEG-silane monolayers were glass microscope slides or Si wafers. To reduce the extent of silane polymerization in solution, leading subsequently to the formation of an uneven multilayer, the preparations were carried out in moisture-controlled conditions. All glassware and substrates were dried in an oven overnight before use. The substrate (glass slide/silicon wafer) was placed in a Schlenk tube sealed with a septum. The tube was purged three times by filling with nitrogen followed by evacuation. Dry toluene was degassed with nitrogen for approximately 20 min. The substrates were then immersed in a 1 mM solution of OEG-silane and left for 2 h. The substrates were rinsed with ethanol, sonicated in toluene for 10 min, and rinsed again with ethanol. Substrates were then dried under a stream of nitrogen, placed under vacuum at 120 °C, and left to anneal for 1 h.

Nanolithography was carried out using two instruments. Patterning using apertured probes was carried out on a home-built parallel near-field lithography instrument, the "Snomipede", that is capable of controlling near-field lithography by up to 16 probes in parallel. The instrument has been described in detail elsewhere.[29] For this instrument, AFM-type probes, consisting of rectangular cantilevers with hollow pyramidal tips at their apexes (WiTec GmbH) were employed. Light from a continuous-wave laser beam (Innova I328, 364 nm, Coherent, Ely, U.K.) was coupled to a SNOM probe, and the probe was traced across the sample to modify lines of adsorbates. For apertureless photocalytic lithography, a WiTec α-SNOM system was used. Standard contact mode AFM probes with force constants from 0.12 to 0.35 N m^{-1} were coated with a 15−20 nm thick Ti layer by thermal evaporation. The coated probes were annealed in air at 450 °C for 30 min to allow formation of a native oxide layer. Annealing likely produces the photocatalytically active anatase phase, and was essential for good lithographic results. The probes were excited by light from an HeCd laser (325 nm, Kimmon IK3202R-D), which was first expanded (to a cross-sectional area of approximately 1 cm^2) and then directed at the sample-probe gap with an angle of incidence of almost zero degrees between the laser beam and the sample surface.

After photocatalytic nanopatterning, the *n*-alkanethiolate self-assembled monolayers were rinsed in ethanol and modified regions were backfilled by dipping the samples for 10 min in a 10 mM solution of either 11-mercaptoundecanoic acid (for dodecanethiol SAMs), or dodecanethiol (for 11-mercaptoundecanoic acid SAMs) for 2h. The samples were then rinsed with clean ethanol and nitrogen dried. After patterning of the OEG-silane films, they were derivatized by exposing them to a 20 mM aqueous solution of AB-NTA for 2 h. The samples were then cleaned with deionized water and blown dry with nitrogen. For attachment of histidine-tagged green fluorescent protein (His-GFP), the samples were first immersed in a 10 mM aqueous solution of nickel sulfate for 5 min to ensure complexation of NTA by Ni^{2+}. The samples were washed thoroughly with deionized water and blown dry with nitrogen with to remove excess Ni^{2+} ions present on surfaces. The samples were then immersed in His-GFP solution diluted with 20 mM Tris buffer in the ratio of 1:20. The surfaces were left immersed in the protein solution for 24 h in a humid chamber. The samples were then gently washed by repeatedly dipping in deionized water and 1 mM aqueous KCl solution and blown dry with a gentle nitrogen flow.

Patterned samples were characterized by atomic force microscopy and lateral force microscopy (LFM) using a Veeco Nanoscope IV Multimode AFM system. For contact mode imaging, silicon nitride probes (Nanoprobes, Veeco) with average spring constants 0.06 or 0.12 N m^{-1} and nominal tip radii between 20 and 60 nm were used. For tapping mode measurements, silicon probes with nominal force constants of 20−80 N m^{-1} were used. GFP patterns were characterized by scanning laser confocal microscopy, using a LSM 510 Meta laser scanning confocal microscope (Carl Zeiss, Welwyn Garden City, U.K.). The samples were mounted in a glycerol/PBS-based antifade solution (Citifluor AF1, Agar Scientific, U.K.) and observed with 40× and 63× oil immersion objectives (numerical apertures of 1.30 and 1.40, respectively). A small drop of immersion oil (Immersol 518 F, Zeiss) was placed on the slide in the center of the lighted area. All fluorescence images were analyzed using Zeiss LSM image browser software.

Conflict of Interest: The authors declare no competing financial interest.

Acknowledgment. The authors thank EPSRC (Grant EP/050271/1), RCUK (Grant EP/C523857/1), and BBSRC (Grant BB/G021546/1) for financial support.

REFERENCES AND NOTES

1. Sagiv, J. Organized Monolayers by Adsorption. 1. Formation and Structure of Oleophobic Mixed Monolayers on Solid Surfaces. *J. Am. Chem. Soc.* **1980**, *102*, 92–98.
2. Netzer, L.; Sagiv, J. A New Approach to Construction of Artificial Monolayer Assemblies. *J. Am. Chem. Soc.* **1983**, *105*, 674–676.
3. Nuzzo, R. G.; Allara, D. L. Adsorption of Bifunctional Organic Disulfides on Gold Surfaces. *J. Am. Chem. Soc.* **1983**, *105*, 4481–4483.
4. Bain, C. D.; Troughton, E. B.; Tao, Y.-T.; Evall, J.; Whitesides, G. M.; Nuzzo, R. G. Formation of Monolayer Films by the Sponaneous Assembly of Organic Thiols from Solution onto Gold. *J. Am. Chem. Soc.* **1989**, *111*, 321–335.
5. Love, J. C.; Estroff, L. A.; Kriebel, J. K.; Nuzzo, R. G.; Whitesides, G. M. Self-Assembled Monolayers of Thiolates on Metals as

a Form of Nanotechnology. *Chem. Rev.* **2005**, *105*, 1103–1170.
6. Piner, R. D.; Zhu, J.; Xu, F.; Hong, S.; Mirkin, C. A. "Dip-Pen" Nanolithography. *Science* **1999**, *283*, 661–663.
7. Ginger, D. S.; Zhang, H.; Mirkin, C. A. The Evolution of Dip-Pen Nanolithography. *Angew. Chem., Int. Ed.* **2004**, *43*, 30–45.
8. Demers, L.; Ginger, D. S.; Park, S.-J.; Li, Z.; Chung, S.-W.; Mirkin, C. A. Direct Patterning of Modified Oligonucleotides on Metals and Insulators by Dip-Pen Nanolithography. *Science* **2002**, *296*, 1836–1838.
9. Lee, K.-B.; Park, S.-J.; Mirkin, C. A.; Smith, J. C.; Mrksich, M. Protein Nanoarrays Generated by Dip-Pen Nanolithography. *Science* **2002**, *295*, 1702–1705.
10. Bullen, D.; Chung, S.-W.; Wang, X.; Zou, J.; Mirkin, C. A.; Liu, C. Parallel Dip-Pen Nanolithography with Arrays of Individually Addressable Cantilevers. *Appl. Phys. Lett.* **2004**, *84*, 789–791.
11. Salaita, K.; Wang, Y.; Fragala, J.; Vega, R. A.; Liu, C.; Mirkin, C. A. Massively Parallel Dip-Pen Nanolithography with 55000-Pen Two-Dimensional Arrays. *Angew. Chem., Int. Ed.* **2006**, *45*, 7220–7223.
12. Huo, F.; Zheng, Z.; Zheng, G.; Giam, L. R.; Zhang, H.; Mirkin, C. A. Polymer Pen Lithography. *Science* **2008**, *321*, 1658–1660.
13. Amro, N. A.; Xu, S.; Liu, G.-Y. Patterning Surfaces Using Tip-Directed Displacement and Assembly. *Langmuir* **2000**, *16*, 3006–3009.
14. Wadu-Mesthrige, K.; Amro, N. A.; Garno, J. C.; Xu, S.; Liu, G.-Y. Fabrication of Nanometer-Sized Protein Patterns Using Atomic Force Microscopy and Selective Immobilization. *Biophys. J.* **2001**, *80*, 1891–1899.
15. Shi, J.; Chen, J.; Cremer, P. S. Sub-100 nm Patterning of Supported Bilayers by Nanoshaving Lithography. *J. Am. Chem. Soc.* **2008**, *130*, 2718–2719.
16. Maoz, R.; Frydman, E.; Cohen, S. R.; Sagiv, J. Constructive Nanolithography: Site-Defined Silver Self-Assembly on Nanoelectrochemically Patterned Monolayer Surfaces. *Adv. Mater.* **2000**, *12*, 424–429.
17. Maoz, R.; Frydman, E.; Cohen, S. R.; Sagiv, J. "Constructive Nanolithography": Inert Monolayers as Patternable Templates for In-Situ Nanofabrication of Metal-Semiconductor-Organic Surface Struscutres—A Generic Approach. *Adv. Mater.* **2000**, *12*, 725–731.
18. Golzhauser, A.; Eck, W.; Geyer, W.; Stadler, V.; Grunze, M. Chemical Nanolithography with Electron Beams. *Adv. Mater.* **2001**, *13*, 803–806.
19. Ballav, N.; Terfort, A.; Zharnikov, M. Fabrication of Mixed Self-Assembled Monolayers Designed for Avidin Immobilization by Irradiation Promoted Exchange Reaction. *Langmuir* **2009**, *25*, 9189–9196.
20. Ballav, N.; Thomas, H.; Winkler, T.; Terfort, A.; Zharnikov, M. Making Protein Patterns by Writing in a Protein-Repelling Matrix. *Angew. Chem., Int. Ed.* **2009**, *48*, 5833–5836.
21. Krakert, S.; Ballav, N.; Zharnikov, M.; Terfort, A. Adjustment of the Bioresistivity by Electron Irradiation: Self-Assembled Monolayers of Oligo(ethyleneglycol)-Terminated Alkanethiols with Embedded Cleavable Group. *Phys. Chem. Chem. Phys.* **2010**, *12*, 507–515.
22. McLellan, J. M.; Geissler, M.; Xia, Y. Edge Spreading Lithography and Its Application to the Fabrication of Mesoscopic Gold and Silver Rings. *J. Am. Chem. Soc.* **2004**, *126*, 10830.
23. Coyer, S. R.; García, A. J.; Delamarche, E. Facile Preparation of Complex Protein Architectures with Sub-100-nm Resolution on Surfaces. *Angew. Chem., Int. Ed.* **2007**, *46*, 6837–6840.
24. Liao, W.-S.; Cheunkar, S.; Cao, H. H.; Bednar, H. R.; Weiss, P. S.; Andrews, A. M. Subtractive Patterning *via* Chemical Lift-Off Lithography. *Science* **2012**, *337*, 1517–1521.
25. Sun, S.; Chong, K. S. L.; Leggett, G. J. Nanoscale Molecular Patterns Fabricated by Using Scanning Near-Field Optical Lithography. *J. Am. Chem. Soc.* **2002**, *124*, 2414–2415.
26. Sun, S.; Leggett, G. J. Generation of Nanostructures by Scanning Near-field Photolithography of Self-Assembled Monolayers and Wet Chemical Etching. *Nano Lett.* **2002**, *2*, 1223–1227.
27. Sun, S.; Leggett, G. J. Matching the Resolution of Electron Beam Lithography by Scanning Near-Field Photolithography. *Nano Lett.* **2004**, *4*, 1381–1384.
28. Leggett, G. J. Light-Directed Nanosynthesis: Near-Field Optical Approaches to Integration of the Top-Down and Bottom-Up Fabrication Paradigms. *Nanoscale* **2012**, *4*, 1840–1855.
29. Ul-Haq, E.; Liu, Z.; Zhang, Y.; Ahmad, S. A. A.; Wong, L.-S.; Armes, S. P.; Hobbs, J. K.; Leggett, G. J.; Micklefield, J.; Roberts, C. J.; et al. Parallel Scanning Near-Field Photolithography: The Snomipede. *Nano Lett.* **2010**, *10*, 4375–4380.
30. Lim, J.-H.; Ginger, D. S.; Lee, K.-B.; Heo, J.; Nam, J.-M.; Mirkin, C. A. Direct-Write Dip-Pen Nanolithography of Proteins on Modified Silicon Oxide Surfaces. *Angew. Chem., Int. Ed.* **2003**, *42*, 2309–2312.
31. Zhou, D.; Wang, X.; Birch, L.; Rayment, T.; Abell, C. AFM Study on Protein Immobilization on Charged Surfaces at the Nanoscale: Toward the Fabrication of Three-Dimensional Protein Nanostructures. *Langmuir* **2003**, *19*, 10557–10562.
32. Falconnet, D.; Pasqui, D.; Park, S.; Eckert, R.; Schift, H.; Gobrecht, J.; Barbucci, R.; Textor, M. Approach to Produce Protein Nanopatterns by Combining Nanoimprint Lithography and Molecular Self-Assembly. *Nano Lett.* **2004**, *4*, 1909–1914.
33. Gu, J.; Yam, C. M.; Li, S.; Cai, C. Nanometric Protein Arrays on Protein-Resistant Monolayers on Silicon Surfaces. *J. Am. Chem. Soc.* **2004**, *126*, 8098–8099.
34. Agheli, H.; Malmstrom, J.; Larsson, E. M.; Textor, M.; Sutherland, D. S. Large Area Protein Nanopatterning for Biological Applications. *Nano Lett.* **2006**, *6*, 1165–1171.
35. Calvacanti-Adam, A., E.; Micoulet, A.; Blümmel, J.; Auernheimer, J.; Kessler, H.; Spatz, J. P. Lateral Spacing of Integrin Ligands Influences Cell Spreading and Focal Adhesion Assembly. *Eur. J. Cell Biol.* **2006**, *85*, 219–224.
36. Zheng, Z.; Daniel, W. L.; Giam, L. R.; Huo, F.; Senesi, A. J.; Zheng, G.; Mirkin, C. A. Multiplexed Protein Arrays Enabled by Polymer Pen Lithography: Addressing the Inking Challenge. *Angew. Chem., Int. Ed.* **2009**, *48*, 7626–7629.
37. Michel, R.; Lussi, J. W.; Csucs, G.; Reviakine, I.; Danuser, G.; Ketterer, B.; Hubbell, J. A.; Textor, M.; Spencer, N. D. Selective Molecular Assembly Patterning: A New Approach to Micro- and Nanochemical Patterning of Surfaces for Biological Applications. *Langmuir* **2002**, *18*, 3281–3287.
38. Maury, P.; Escalante, M.; Péter, M.; Reinhoudt, D. N.; Subramaniam, V.; Huskens, J. Creating Nanopatterns of His-Tagged Proteins on Surfaces by Nanoimprint Lithography Using Specific NiNTA-Histidine Interactions. *Small* **2007**, *3*, 1584–1592.
39. Escalante, M.; Lenferink, A.; Zhao, Y.; Tas, N.; Huskens, J.; Hunter, C. N.; Subramaniam, V.; Otto, C. Long-Range Energy Propagation in Nanometer Arrays of Light Harvesting Antenna Complexes. *Nano Lett.* **2010**, *10*, 1450–1457.
40. Alang Ahmad, S. A.; Wong, L. S.; ul Haq, E.; Hobbs, J. K.; Leggett, G. J.; Micklefield, J. Protein Micro- and Nanopatterning Using Aminosilanes with Protein-Resistant Photolabile Protecting Groups. *J. Am. Chem. Soc.* **2011**, *133*, 2749–2759.
41. Harris, J. M. *Poly(Ethylene Glycol) Chemistry: Biochemical and Biomedical Applications*; Plenum: New York, 1992.
42. Pale-Grosdemange, C.; Simon, E. S.; Prime, K. L.; Whitesides, G. M. Formation of Self-Assembled Monolayers by Chemisorption of Derivatives of Oligo(Ethylene glycol) of Structure $HS(CH_2)_{11}(OCH_2CH_2)_mOH$ on Gold. *J. Am. Chem. Soc.* **1991**, *113*, 12–20.
43. Prime, K. L.; Whitesides, G. M. Self-Assembled Organic Monolayers: Model Systems for Studying Adsorption of Proteins at Surfaces. *Science* **1991**, *252*, 1164–1167.
44. Ostuni, E.; Chapman, R. G.; Holmlin, E. R.; Takayama, S.; Whitesides, G. M. A Survey of Structure−Property Relationships of Surfaces that Resist the Adsorption of Protein. *Langmuir* **2001**, *17*, 5605–5620.

45. Lopez, G. P.; Albers, M. W.; Schreiber, S. L.; Carroll, R.; Peralta, E.; Whitesides, G. M. Convenient Methods for Patterning the Adhesion of Mammalian Cells to Surfaces using Self-Aseembled Monolayers of Alkanethiolates on Gold. *J. Am. Chem. Soc.* **1993**, *115*, 5877–5878.
46. Lopez, G. P.; Biebuyck, H. A.; Haerter, R.; Kumar, A.; Whitesides, G. M. Fabrication and Imaging of Two-Dimensional Patterns of Proteins Adsorbed on Self-Assembled Monolayers by Scanning Electron Microscopy. *J. Am. Chem. Soc.* **1993**, *115*, 10774–10781.
47. Singhvi, R.; Kumar, A.; Lopez, G. P.; Stephanopoulos, G. N.; Wang, D. I. C.; Whitesides, G. M.; Ingber, D. E. Engineering Cell Shape and Function. *Science* **1994**, *264*, 696–698.
48. Michel, R.; Pasche, S.; Textor, M.; Castner, D. G. Influence of PEG Architecture on Protein Adsorption and Conformation. *Langmuir* **2005**, *21*, 12327–12332.
49. López, G. P.; Ratner, B. D.; Tidwell, C.; Haycox, C.; Rapoza, R.; Horbett, T. Glow Discharge Plasma Deposition of Tetraethylene Glycol Dimethyl Ether for Fouling-Resistant Biomaterial Surfaces. *J. Biomed. Mater. Res.* **1991**, *26*, 415–439.
50. Shen, M.; Pan, Y. V.; Wagner, M. S.; Hauch, K. D.; Castner, D. G.; Ratner, B. D.; Horbett, T. A. Inhibition of Monocyte Adhesion and Fibrinogen Adsorption on Glow Discharge Plasma Deposited Tetraethylene Glycol Dimethyl Ether. *J. Biomater. Sci., Polym. Ed.* **2001**, *12*, 961–978.
51. Hurley, C. R.; Ducker, R. E.; Leggett, G. J.; Ratner, B. D. Fabrication of Submicrometer Biomolecular Patterns by Near-Field Exposure of Plasma-Polymerized Tetraglyme Films. *Langmuir* **2010**, *26*, 10203–10209.
52. Ma, H.; Li, D.; Sheng, X.; Zhao, B.; Chilkoti, A. Protein Resistant Polymer Brushes on Silicon Oxide by Surface Initiated Atom Transfer Radical Polymerization. *Langmuir* **2006**, *22*, 3751–3756.
53. Ma, H.; Wells, M., Jr.; T., P. B.; Chilkoti, A. Surface Initiated Polymerization of Nonfouling Polymer Brushes of Oligoethylene Glycol Methacrylate on Gold. *Adv. Funct. Mater.* **2006**, *16*, 640–648.
54. Hucknall, A.; Simnick, A. J.; Hill, R. T.; Chilkoti, A.; Garcia, A.; Johannes, M. S.; Clark, R. L.; Zauscher, S.; Ratner, B. D. Versatile Synthesis and Micropatterning of Nonfouling Polymer Brushes on the Wafer Scale. *Biointerphases* **2009**, *4*, FA50–FA57.
55. Montague, M.; Ducker, R. E.; Chong, K. S. L.; Manning, R. J.; Rutten, F. J. M.; Davies, M. C.; Leggett, G. J. Fabrication of Biomolecular Nanostructures by Scanning Near-Field Photolithography of Oligo(ethylene glycol) Terminated Self-Assembled Monolayers. *Langmuir* **2007**, *23*, 7328–7337.
56. Kobayashi, Y.; Sakai, M.; Ueda, A.; Maruyama, K.; Saiki, T.; Suzuki, K. Writing and Reading Methodology for Biochips with Sub-100-nm Chemical Patterns Based on Near-Field Scanning Optical Microscopy. *Anal. Sci.* **2008**, *24*, 571–576.
57. Reynolds, N. P.; Tucker, J. D.; Davison, P. A.; Timney, J. A.; Hunter, C. N.; Leggett, G. J. Site-Specific Immobilization and Micrometer and Nanometer Scale Photopatterning of Yellow Fluorescent Protein on Glass Surfaces. *J. Am. Chem. Soc.* **2009**, *131*, 896–897.
58. Wang, R.; Hashimoto, K.; Fujishima, A.; Chikuni, M.; Kojima, E.; Kitamura, A.; Shimohigoshi, M.; Watanabe, T. Light-Induced Amphiphilic Surfaces. *Nature* **1997**, *388*, 431–432.
59. Haick, H.; Paz, Y. Remote Photocatalytic Activity as Probed by Measuring the Degradation of Self-Assembled Monolayers Anchored Near Microdomains of Titanium Dioxide. *J. Phys. Chem. B* **2001**, *105*, 3045–3054.
60. Haick, H.; Paz, Y. "Dark" Photocatalysis: The Degradation of Organic Molecules Anchored to Dark Microdomains of Titanium Dioxide. *ChemPhysChem* **2003**, *4*, 617–620.
61. Blondiaux, N.; Zurcher, S.; Liley, M.; Spencer, N. D. Fabrication of Multiscale Surface-Chemical Gradients by Means of Photocatalytic Lithography. *Langmuir* **2007**, *23*, 3489–3494.
62. Tizazu, G.; Adawi, A.; Leggett, G. J.; Lidzey, D. G. Photopatterning, Etching, and Derivatization of Self-Assembled Monolayers of Phosphonic Acids on the Native Oxide of Titanium. *Langmuir* **2009**, *25*, 10746–10753.
63. Nakata, K.; Nishimoto, S.; Yuda, Y.; Ochiai, T.; Murakami, T.; Fujishima, A. Rewritable Superhydrophilic-Superhydrophobic Patterns on a Sintered Titanium Dioxide Substrate. *Langmuir* **2010**, *26*, 11628–11630.
64. Tizazu, G.; El-Zubir, O.; Brueck, S. R. J.; Lidzey, D. G.; Leggett, G. J.; Lopez, G. P. Large Area Nanopatterning of Alkylphosphonate Self-Assembled Monolayers on Titanium Oxide Surfaces by Interferometric Lithography. *Nanoscale* **2011**, *3*, 2511–2516.
65. Nishimoto, S.; Kubo, A.; Zhang, X.; Liu, Z.; Taneichi, N.; Okui, T.; Murakami, T.; Komine, T.; Fujishima, A. Novel Hydrophobic/Hydrophilic Patterning Process by Photocatalytic Ag Nucleation on TiO_2 Thin Film and Electroless Cu Deposition. *Appl. Surf. Sci.* **2008**, *254*, 5891–5894.
66. Paz, Y. Self-Assembled Monolayers and Titanium Dioxide: From Surface Patterning to Potential Applications. *Beilstein J. Nanotechnol.* **2011**, *2*, 845–861.
67. Zhang, L.; Diao, S.; Nie, Y.; Yan, K.; Liu, N.; Dai, B.; Xie, Q.; Reina, A.; Kong, J.; Liu, Z. Photocatalytic Patterning and Modification of Graphene. *J. Am. Chem. Soc.* **2011**, *133*, 2706–2713.
68. Ducker, R. E.; Janusz, S. J.; Sun, S.; Leggett, G. J. Photochemical Introduction of Nanopatterned Protein-Binding Functionalities to Oligo(Ethylene Glycol) Terminated Self-Assembled Monolayers. *J. Am. Chem. Soc.* **2007**, *129*, 14842–14843.
69. Alang-Ahmad, S. A.; Hucknall, A.; Chilkoti, A.; Leggett, G. J. Protein Patterning by UV-induced Photodegradation of Poly(oligo(ethylene glycol)methacrylate) Brushes. *Langmuir* **2010**, *26*, 9937–9942.
70. Tizazu, G.; el Zubir, O.; Patole, S.; McLaren, A.; Vasilev, C.; Mothersole, D.; Adawi, A.; Hunter, C. N.; Lidzey, D.; Lopez, G.; et al. Micrometer and Nanometer Scale Photopatterning of Proteins on Glass Surfaces by Photodegradation of Films Formed from Oligo(ethylene glycol) Terminated Silanes. *Biointerphases* **2012**, *7*, 1–9.
71. Prasher, D. C.; Eckenrode, V. K.; Ward, W. W.; Prendergast, F. G.; Cormier, M. J. Primary Structure of the Aequorea Victoria Green-Fluorescent Protein. *Gene* **1992**, *111*, 229.
72. Tsien, R. Y. The Green Fluorescent Protein. *Annu. Rev. Biochem.* **1998**, *67*, 509.